



# Spin and orbital Yu-Shiba-Rusinov states and delocalization control of magnetic order in parallel double quantum dot Josephson junctions

Meng-Ya Ma <sup>1</sup>, Rui-Cong Xu,<sup>2</sup> Wei-Jiang Gong,<sup>1</sup> and Guang-Yu Yi <sup>1,\*</sup>

<sup>1</sup>College of Sciences, *Northeastern University*, Shenyang 110819, China

<sup>2</sup>College of Medicine and Biological Information Engineering, *Northeastern University*, Shenyang 110819, China



(Received 19 May 2024; revised 13 August 2024; accepted 22 August 2024; published 3 September 2024)

With the help of the numerical renormalization group method, we theoretically investigate the Josephson phase transition and the Yu-Shiba-Rusinov (YSR) states in parallel-coupled double quantum dot (QD) Josephson junctions. The interplay of competition and cooperation of multiple energy scales within the system results in distinct impacts on the  $0-\pi$  transition behavior and the evolution of YSR states when the QDs are in the half-filled case. This arises from the relative variation in the strengths of the interdot antiferromagnetic correlation and the Ruderman-Kittel-Kasuya-Yosida interaction. In addition, when the interdot coupling coefficient  $t_{12}$  is fixed, by adjusting the phase difference between superconducting electrodes, we found that the magnetic order of two QDs and the YSR subgap states can be controlled in a delocalized manner. Our research explores the complexities of electron correlation effects in Josephson junctions, providing unique insights into the construction and regulation of superconducting nanodevices and quantum bits in the future. Furthermore, the system's spin and orbital degrees of freedom can be manipulated to satisfy the SU(4) symmetry by adjusting the QD levels and other parameters. An orbital YSR state is induced by a pseudospin-flip process involving pseudospins and quasiparticles outside the superconducting gap. We provide a detailed analysis of the various physical mechanisms underlying the emergence of spin and orbital YSR states through the application of an external magnetic field.

DOI: [10.1103/PhysRevB.110.125105](https://doi.org/10.1103/PhysRevB.110.125105)

## I. INTRODUCTION

Semiconductor quantum dots (QDs) are artificial mesoscopic systems widely used to study electron strong correlation effects due to their strong Coulomb interaction and adjustable system parameters [1–5]. The Kondo effect is a typical many-body correlation effect, which was first discovered in diluted magnetic alloys containing local magnetic impurities. Below the Kondo temperature  $T_K$ , it exhibits the anomalous behavior of the low-temperature resistivity [6–9]. Unlike in traditional macroscopic metal hosts, Kondo physics in QDs can be investigated in a controllable and precise way.

By embedding QDs between two superconductors (SCs), a mesoscopic Josephson junction can be assembled. The strong electron interaction within the system drives the well-known Josephson phase transition [10–13]. If the Kondo temperature  $T_K$  is much larger than the superconducting-pairing potential  $\Delta$ , the Josephson current follows the functional form of  $I = I_C \sin(\Delta\varphi)$ , where  $I_C$  is the critical current and  $\Delta\varphi$  is the inter-SC phase difference, leading to  $0$ -junction behavior. Alternatively, if the Josephson junction enters its  $\pi$  phase [14], it exhibits a negative value in another functional form of  $I = I_C \sin(\Delta\varphi + \pi)$ .

In the QD-SC junction, a subgap excitation state known as the Yu-Shiba-Rusinov (YSR) state can be induced [15–22]. The excitation energies of the YSR states in this setup can be tuned by gate voltages or other system param-

eters. During the  $0-\pi$  phase transition, if the Kondo correlation is weak, the ground state will be the standard BCS wave function with all single-particle states forming Cooper pairs accompanied by an unscreened impurity magnetic moment. Conversely, increasing the Kondo correlation will destroy the superconducting pairing potential due to impurity magnetic moment. Under this condition, paired YSR states can appear near the superconducting energy gap and undergo zero-energy crossover near the quantum phase transition point where  $T_K \sim \Delta$ , with singlet and doublet of different parities crossing at the Fermi surface [18].

In the impurity and SC composite systems, another type of subgap bound state is known as the Majorana bound state (MBS) [23–28]. In recent years, due to its potential applications in quantum fault-tolerant computation, it has received much attention from researchers in both theoretical and experimental aspects. Previous studies have shown that such novel topological-superconductor (TSC) electronic states can be realized in quantum wires made of materials with strong spin-orbit coupling in the proximity of an  $s$ -wave superconductor. External magnetic fields are applied to break time-reversal symmetry to produce effectively spinless electrons with  $p$ -wave superconducting pairing, leading to the effective realization of the one-dimensional Kitaev model, and so MBSs can emerge at the end of the wire [26–28].

Recent reports have indicated that the MBSs can also be realized by magnetic adatoms chains on the surface of  $s$ -wave SCs, without the need for spin-orbit interaction [29–32]. When these adatoms are organized into one-dimensional chains, their spins spontaneously align in a helical order due

\*Contact author: [ygy\\_neu@163.com](mailto:ygy_neu@163.com)

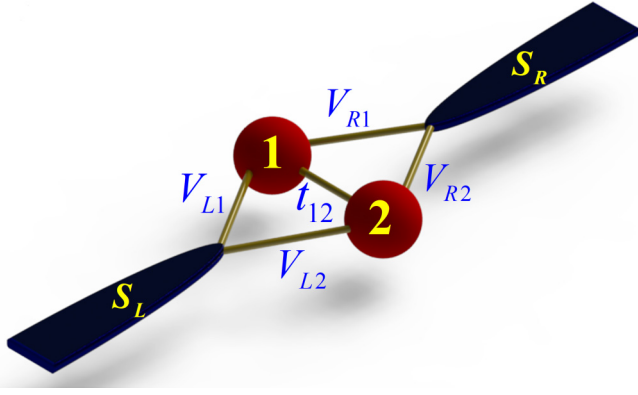


FIG. 1. Schematic diagram of a parallel DQD Josephson junction.

to the Ruderman-Kittel-Kasuya-Yosida (RKKY) interaction [33]. The polarized YSR states approach and hybridize with each other to form a subgap band, mimicking anomalous  $p$ -wave correlations and allowing for the possibility of forming MBSs.

To understand the physical mechanism of the YSR state and MBS transition, researchers have focused on studying YSR states formed in a few magnetic atoms deposited on superconducting substrates [34–39]. It was found that the RKKY interaction strength between magnetic diatoms can be altered, and the splitting and merging of a pair of spin-related YSR states can be adjusted [38].

The parallel double quantum dot (DQD) molecules represent the smallest system with RKKY interaction among various QD structures. The characteristic energies associated with electron correlation effects in this system, such as the Kondo temperature  $T_K$ , superconducting-pairing potential  $\Delta$ , and characteristic temperature  $T_F$  of RKKY interaction, give rise to competition and cooperation mechanisms. Additionally, aside from spin, the pseudospin resulting from orbital degrees of freedom also plays a significant role in this system. Therefore, the Kondo correlation involves both spin and pseudospin-flip events, and their strong mixing results in spin-orbit Kondo properties that are distinctly different from an ordinary SU(2) spin-Kondo effect which only involves spin-flip events [40–43].

Recently, Kürtössy *et al.* fabricated DQD molecules utilizing the parallel InAs nanowires, which form a parallel structure through the connection of each Ti/Al superconductor lead. They discovered the emergence of Andreev molecular states. By independently adjusting the energy levels of different QDs in the upper and lower arms, they observed the shifts of the spectral line positions and the changes in the shape of YSR states [44].

We are motivated by the aforementioned experimental results, and it is a natural idea to incorporate an interdot coupling coefficient in a parallel DQD system, as illustrated in Fig. 1. We employ the numerical renormalization group (NRG) method to investigate the Josephson current, spin correlation function, and thermodynamic quantities such as entropy in this system. The calculation results indicate that adjusting the interdot coupling coefficient can not only alter the interdot antiferromagnetic coupling between QDs, but also

impact the  $0$ - $\pi$  phase transition behavior of Josephson junctions; furthermore, while keeping  $t_{12}$  unchanged, adjusting parameters such as the phase difference of superconducting electrodes can also alter the relative magnitudes of RKKY interaction strength and the interdot antiferromagnetic correlation strength in the system. Finally, we explore the potential application of this phase transition mechanism in controlling the magnetic order of QDs, which can be applied to construct and regulate the superconducting nanodevices [45,46] and quantum bits in the future.

The rest of this paper is organized as follows. In Sec. II, we introduce the model Hamiltonian of the system and the method of calculation. The numerical results are presented and discussed in Sec. III. Finally, we give the summary in Sec. IV.

## II. MODEL AND THEORY

The parallel Josephson junction that we consider is illustrated in Fig. 1. Its Hamiltonian is written as  $H = H_S + H_{\text{DQD}} + H_T$ . The first term is the Hamiltonian of the SCs within the standard BCS mean-field approximation. It takes the form

$$H_S = \sum_{\alpha k \sigma} \varepsilon_{\alpha, k} a_{\alpha, k \sigma}^\dagger a_{\alpha, k \sigma} + \sum_{\alpha k} (\Delta e^{i\varphi_\alpha} a_{\alpha, k \downarrow} a_{\alpha, -k \uparrow} + \Delta e^{-i\varphi_\alpha} a_{\alpha, -k \uparrow} a_{\alpha, k \downarrow}^\dagger). \quad (1)$$

$\varphi_\alpha$  and  $\Delta$  are superconducting phase and energy gap, respectively, with  $\alpha = L, R$ .  $a_{\alpha, k \sigma}^\dagger$  ( $a_{\alpha, k \sigma}$ ) is the operator that creates (annihilates) an electron with energy  $\varepsilon_{\alpha, k}$  for SC- $\alpha$ , where  $k$  is the momentum quantum number of the free conduction electrons. Next,  $H_{\text{DQD}}$ , modeling the Hamiltonian for the two QDs, reads as

$$H_{\text{DQD}} = \sum_{\sigma, j=1}^2 \varepsilon_j d_{j\sigma}^\dagger d_{j\sigma} + \sum_{j=1}^2 U_j n_{j\uparrow} n_{j\downarrow} + \sum_{\sigma} (t_{12} d_{1\sigma}^\dagger d_{2\sigma} + \text{H.c.}). \quad (2)$$

$d_{j\sigma}^\dagger$  ( $d_{j\sigma}$ ) is the operator to create (annihilate) an electron with energy  $\varepsilon_j$  and spin  $\sigma$  in QD- $j$  ( $j = 1, 2$ ).  $t_{12}$  is the interdot coupling coefficient, and  $U_j$  indicates the strength of intradot Coulomb repulsion in the corresponding QD. The last term of  $H$  denotes the coupling between the QDs and SCs. For our considered system, it can be directly written as

$$H_T = \sum_{\alpha, k, j, \sigma} (V_{\alpha k j} a_{\alpha, k \sigma}^\dagger d_{j\sigma} + \text{H.c.}). \quad (3)$$

$V_{\alpha k j}$  describes the QD-lead coupling coefficient.

Due to the advancement of nanotechnology, the theoretical model in our research can now be fabricated in the laboratory. Recently, Vekris *et al.* have employed molecular beam epitaxy to grow two closely spaced InAs nanowires on a Si/SiOx substrate [47]. Subsequently, a scheme was employed to combine *in situ* deposition of superconductor Al on the nanowires' surface with partial chemical etching in order to connect the nanowires into parallel mesoscopic Josephson junctions. QDs are formed when the two bare nanowires are brought near depletion with the use of the individual side-gate voltages.

The side gates are also utilized as plunger gates for the QDs to adjust their energy levels. Furthermore, the use of finger gates array technology allows for convenient adjustment of the strength of the interdot coupling coefficient in double quantum dots [48].

When there is a certain phase difference between superconducting electrodes, a Josephson current will be driven in the system. With respect to such a junction, the supercurrent properties can be evaluated by the following formula:

$$I_J = \frac{2e}{\hbar} \frac{\partial \langle H \rangle}{\partial \varphi} = \frac{2e}{\hbar} \frac{\partial F}{\partial \varphi}. \quad (4)$$

$\varphi = \varphi_L - \varphi_R$  is the superconducting phase difference between the two SCs.  $F$  represents the free energy of the Josephson junction. At the zero-temperature limit,  $F$  will be reduced into the ground-state (GS) energy of this junction. Accordingly, the zero-temperature current expression can be simplified to be

$$I_J = \frac{2e}{\hbar} \frac{\partial E_{\text{GS}}}{\partial \varphi}. \quad (5)$$

Note that in such a structure, the GS determination is a challenging task that usually requires one appropriate approximation scheme, such as the mean-field approximation and zero-bandwidth (ZBW) approximation [49,50]. However, in comparison with these methods, the NRG method is more accurate to reflect the properties of the GS energy [51–53]. Recently, Estrada Saldaña conducted a study on the  $0-\pi$  transition phenomenon in serial DQDs. They combined several theoretical methods such as NRG and ZBW approximation to numerically calculate the current and phase diagrams, and compared them with experimental results for validation [54]. Therefore, we will perform the NRG method to calculate the ground-state energy and related physical quantities such as current. For the convenience of calculation, we would like to take some simplifications as follows. Assuming that the two SCs are identical ( $\varepsilon_{\alpha k} = \varepsilon_k$  and  $\Delta_\alpha = \Delta$ ), except for a finite phase difference  $\varphi$ . Without loss of generality, we put  $\varphi_L = -\varphi_R = \varphi/2$ . For the dot-lead tunneling coupling  $V_{\alpha k j}$ , we only consider the case of symmetric junction with  $V_{\alpha k j} = V$ , so the dot-lead coupling strength can be defined as  $\Gamma = \pi V^2 \rho_0$  ( $\rho_0$  is the density of states of the superconducting electrode in normal state). In this paper, we take the value  $\Gamma = 0.04D$ , where  $D$  represents the bandwidth of the superconducting electrodes, we set  $D = 1$  as the global energy unit. In experiments, the strength of the coupling coefficient  $\Gamma \sim 1$  meV/ $h$  ( $h$  is Planck constant). As for the value of  $U$ , since we are mainly concerned with the behavior of the system in the Kondo region, specifically focusing on the superconducting phase transition properties when  $U/\Gamma \gg 1$ , we set  $U/D = 0.8$ . Additionally, different superconducting lead materials have varying  $\Delta$ . For example, in the case of double-layered Ti/Al material  $\Delta \approx 0.14$  meV, but for Pb electrodes  $\Delta \approx 1.3$  meV [55–57]. Therefore, unless otherwise specified, we assume  $\Delta/D = 0.06$  throughout the entire study. With the NRG iterative diagonalization process, we retain the 3000 quantum states with the lowest energy. To improve the accuracy of the results, the  $z$ -averaging method is used to eliminate errors between odd and even iterations [58].

### III. NUMERICAL RESULTS AND DISCUSSIONS

Through calculations using the NRG method, we discovered that certain fixed points of the QD system's group flow correspond to different numbers of electronic microscopic states  $W$ . The relationship between the QD's entropy  $\mathcal{S}_{\text{QD}}$  of the whole system and its number of microstates is given by  $\mathcal{S}_{\text{QD}} = \ln W$  (assuming the Boltzmann constant  $k_B$  is 1). With the NRG iterative diagonalization progresses, the system temperature gradually decreases, resulting in a decrease of the corresponding degree of freedom (the number of microscopic states). Therefore, we can study the changes of the number of microscopic states through the curves of QD's entropy. The relationship between the QD's contribution to the system's entropy and temperature can be expressed as

$$\mathcal{S}_{\text{QD}}(T) = \frac{(E - F)}{T} - \frac{(E - F)_0}{T}. \quad (6)$$

Subscript 0 denotes the QD-absent situation,  $E = \langle H \rangle = \text{Tr}[H e^{-H/(k_B T)}]$  with  $F = -k_B T \ln \text{Tr}[e^{-H/(k_B T)}]$  being the system's free energy. Because the YSR state in the superconducting gap can be reflected in the peak of corresponding QD spectral function, so we consider the spectral function of QD defined by

$$A_d(\omega) = -\frac{1}{\pi} \text{Im} G_d(\omega). \quad (7)$$

$G_d(\omega)$  represents the Fourier form of the retarded Green's function of QD.

#### A. $0-\pi$ phase transition and YRS states evolution caused by multiple energy competition

In Fig. 2(a), we first plot the entropy of the system as a function of the temperature for various  $t_{12}$ . Since we focus on the electron correlation effect when QD-1 and QD-2 are single occupied, we define the QD energy level as the electron-hole symmetry point, i.e.,  $\varepsilon_j = -U/2$ . It can be seen that with the decrease of temperature, the entropy flow curves of the system gradually decrease from  $4 \ln 2$ . This is because when the temperature is high, the QDs are independent, which we call the free orbital region (FOR). Namely, the four states, i.e., empty occupied  $|0\rangle$ , single occupied  $|\uparrow\rangle$  or  $|\downarrow\rangle$ , and double-occupied  $|\uparrow\downarrow\rangle$  appear with equal probability. So  $W = 4^2$  states exist in the two QDs and entropy approaches its initial value  $\mathcal{S}_{\text{QD}} = \ln W = 2 \ln 4$ . With the NRG iteration, the temperature gradually decreases, it is found that corresponding to different  $t_{12}$ , the entropy curve evolves into two different horizontal lines. Specifically, when  $t_{12}$  is relatively small ( $t_{12} = 0.01$  and  $0.04$ ), the entropy curve finally reaches  $\mathcal{S}_{\text{QD}} = \ln 3$ , and then no longer decreases. From  $\mathcal{S}_{\text{QD}} = \ln W = \ln(2\tilde{S} + 1)$ , we can see that the effective total spin of the DQDs  $\tilde{S} = 1$ . At the same time, we plot the curves of interdot spin correlation  $\langle S_1 S_2 \rangle$  as a function of temperature in Fig. 2(b). It can be found that when  $t_{12}$  is relatively small,  $\langle S_1 S_2 \rangle$  has a positive value of about 0.2. It can be shown that the spin correlation between QDs is ferromagnetic. We can assume that this is due to small  $J_{\text{AF}} \approx 4t_{12}^2/U$  is much lower than exchange coupling coefficient  $J_{\text{RKKY}} = 64\Gamma^2/(\pi^2 U)$  of the RKKY interaction. When  $\varepsilon_j = -U/2$ , the QDs are both half-filled and the electrons in the two dots maintain a strong ferromagnetic tendency under

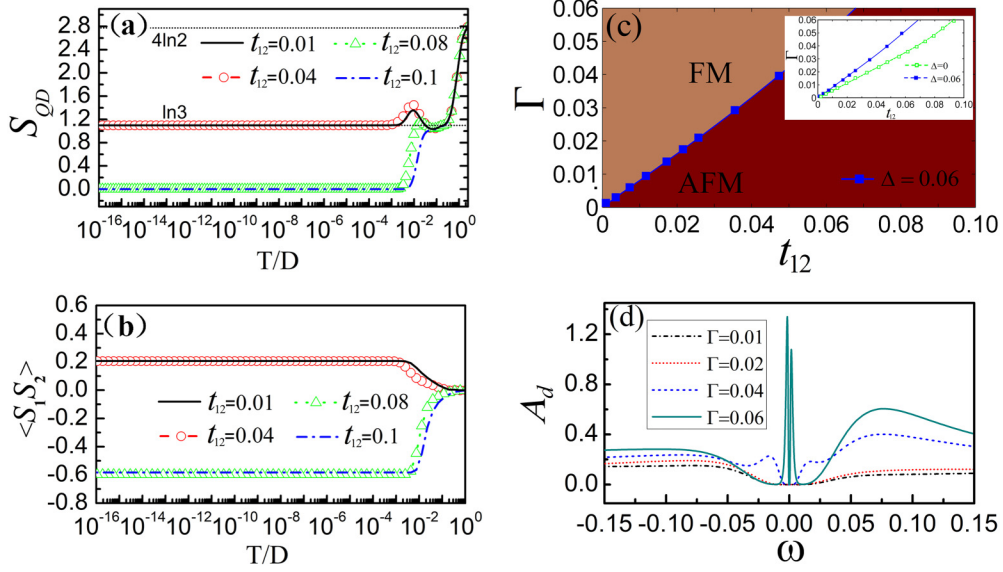


FIG. 2. (a) Temperature dependence of the entropy and (b) the interdot spin correlation function  $\langle S_1 S_2 \rangle$  with various  $t_{12}$ . (c) Magnetic phase diagram in the  $(t_{12}, \Gamma)$  plane for various  $\Delta$ . (d) Spectral function curves of QDs for different values of  $\Gamma$ . The system parameters are taken to be  $\varepsilon_j = -U/2$ ,  $\varphi = \pi/2$ .

the RKKY mechanism caused by the external metal electrode. When  $t_{12}$  gradually increases, the interdot antiferromagnetic exchange becomes the dominant factor. It can be seen that when  $t_{12} = 0.08$  and  $0.1$ , the final value of entropy curve of the system is 0. So the effective total spin is  $\tilde{S} = 0$  and the corresponding spin correlation curve  $\langle S_1 S_2 \rangle$  has a value of approximately  $-0.6$ . These results indicate that in this case the QDs exhibit strong antiferromagnetic relationship, two QDs form a local antiferromagnetic spin singlet.

From the above discussion, it can be inferred that the ferromagnetic and antiferromagnetic phase transition between QDs is predominantly governed by a pair of competing energies, namely, the interdot antiferromagnetic exchange coefficient  $J_{AF}$  and the RKKY interaction  $J_{RKKY}$ . This competition between them induces a triplet-singlet transition at the critical point. For our model, the two localized electrons in the parallel QDs generate the RKKY interaction, which is mediated by the itinerant electrons of the leads. Utilizing Rayleigh-Schrödinger perturbation theory, to the fourth order in  $V$ , the exchange coefficient of the RKKY interaction between QDs can be expressed as [59,60]

$$J_{RKKY} \propto U(\rho_0 J_K)^2 = 64\Gamma^2/(\pi^2 U). \quad (8)$$

Similarly, up to the second order in  $t_{12}$ , the interdot antiferromagnetic exchange coefficient can be expressed as [see Eq. (A5)]

$$J_{AF} = 2t_{12}^2 \left[ \frac{1}{U_1 - U_{12} + (\varepsilon_1 - \varepsilon_2)} + \frac{1}{U_2 - U_{12} - (\varepsilon_1 - \varepsilon_2)} \right], \quad (9)$$

where  $U_{12}$  refers to the interdot Coulomb interaction. When  $U_{12} \rightarrow 0$ ,  $U_j = U$ , and  $\varepsilon_j = -U/2$ , then, Eq. (9) can be simplified as

$$J_{AF} \approx 4t_{12}^2/U. \quad (10)$$

Based on Eqs. (8) and (10), for the case of  $\Gamma = 0.04$ , as  $t_{12}$  increases to  $0.05$ ,  $J_{RKKY} \sim J_{AF}$ . Correspondingly, the spin correlation curve  $\langle S_1 S_2 \rangle$  will experience a ferromagnetic-antiferromagnetic transition at the critical point, as plotted in Figs. 2(a) and 2(b).

Due to the competitive relationship between  $\Delta$  and  $J_K$ , comparing Eqs. (8) and (10),  $\Delta$  has an indirect inhibitory effect on  $J_{RKKY}$  but does not affect  $J_{AF}$ . This new energy scale  $\Delta$  inevitably affects the AFM-FM phase transition process. To understand this behavior, the schematic phase diagram in the parameter space  $(t_{12}, \Gamma)$  is shown in Fig. 2(c). Additionally, its inset illustrates the influence of different  $\Delta$  values on the AFM-FM phase transition boundary. Compared to the case of  $\Delta = 0$ , superconducting pairing potential can suppress the RKKY interaction. It can be observed that, under the same conditions of  $\Gamma$ , increasing the value of  $\Delta$  causes the phase boundary to shift towards the direction with smaller  $t_{12}$ .

In Fig. 2(d), we present the spectral functions of the QD for different values of  $\Gamma$  when  $t_{12} = 0.04$ . When  $\Gamma \leq 0.02$ , there is no YSR peak within the range of  $-\Delta < \omega < \Delta$ . This can be explained as follows. The position of peaks can be given by the binding energy formula

$$E_b^\pm = \pm \Delta \frac{(1 - \tilde{J}^2)}{(1 + \tilde{J}^2)}, \quad (11)$$

where  $\tilde{J}$  is the effective scattering potential in the Kondo impurity model [61]. As  $\Gamma$  decreases to 0,  $\tilde{J} \rightarrow 0$ . So, one can see that peaks gradually merge into the superconducting gap edges. As  $\Gamma$  increases, the DQD transitions from antiferromagnetic to ferromagnetic and, at the same time, two YSR peaks gradually appear in the spectral function curves. With further increase of  $\Gamma$ , the Kondo temperature of the system increases, causing the two YSR peaks to approach each other and cross zero energy. This implies that the system is undergoing a transition from doublet to Kondo singlet.

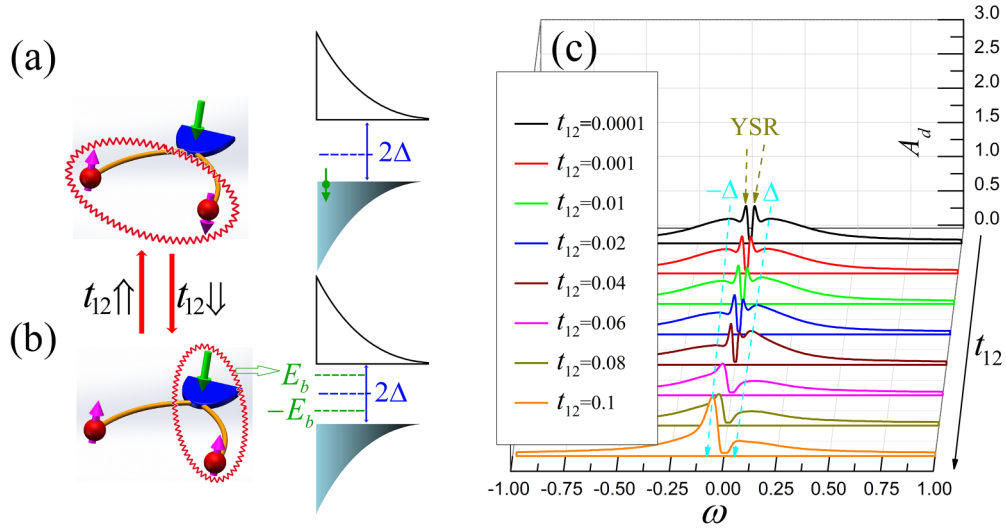


FIG. 3. (a), (b) As  $t_{12}$  increases (decreases), the DQDs transition from ferromagnetic (antiferromagnetic) to antiferromagnetic (ferromagnetic). (c) The evolution of spectral function curve of the QDs with increasing  $t_{12}$ , the system parameters are the same as in Fig. 2.

The above discussion allows us to make the conclusion that the magnetic order of QDs can be dynamically adjusted by changing the coupling coefficient  $t_{12}$ , and this goal can be achieved by adjusting the gate voltage between QDs [22,48]. In Figs. 3(a) and 3(b), we draw a schematic diagram of different spin correlation states between the QDs by adjusting the coefficient  $t_{12}$ . In order to investigate the evolution of YSR states in the QDs system with the variation of spin correlation states, in Fig. 3(c), we plot the spectral function curves of the QD for various  $t_{12}$ . It can be observed that when  $t_{12}$  is relatively small, the spectral function exhibits four symmetric peaks. The two outer peaks have relatively flat shapes and are located at  $\omega = \pm\Delta$ , indicating the value of the superconducting gap. Correspondingly, the two sharp inner peaks in the gap correspond to the YSR states. This is due to the fact that when  $t_{12}$  is small, the presence of the local magnetic moment  $S$  of the QDs forms an equivalent magnetic field  $JS$ , thereby suppressing the formation of superconducting Cooper pairs. Meanwhile, the single-occupied electronic state of the QDs and the quasiparticle states in the SCs form the subgap state, namely, the YSR singlet. As  $t_{12}$  gradually increases, the two single occupying electrons in DQDs tend to form localized antiferromagnetic singlet instead of YSR singlet with the quasiparticles in the superconducting electrode, resulting in the disappearance of YSR state peaks, as shown in Fig. 3(c). This physical mechanism is consistent with the evolution trend reflected by the entropy and spin correlation curves in Figs. 2(a) and 2(b).

Recently, Ding *et al.* manipulated multiple Gd atoms arranged on the surface of bismuth (Bi) superconducting thin films using scanning tunneling microscopy (STM) probe technology, and observed the band structure of YSR states within the superconductor gap [38]. By adjusting parameters such as atomic distance, spin-orbit coupling strength, and surface magnetic anisotropy, the researchers demonstrated the relationship between the tunability of spin-exchange interactions and the precise control of YSR state hybridization. For parallel DQDs, the coefficient  $J_{AF}$  can be adjusted using finger gates array technology. By adjusting the relative strengths of

the exchange coefficients  $J_{RKKY}$  and  $J_{AF}$ , we can manipulate the hybrid structure of YSR states, potentially leading to a topological Kondo phase transition in a controlled system with complex spin structures. Therefore, it can be inferred from the above that in larger systems such as QD arrays, researchers have the potential to utilize the high tunability of QD platforms to create well-defined helical spin states and generate MBSs at their ends. This will pave the way for future possibilities in constructing TSC systems based on QDs [62,63].

Next, in order to investigate the effect of SCs on the Josephson phase transition, we can adjust the value of the superconducting gap  $\Delta$  to induce the occurrence of  $0-\pi$  transition phenomenon in this system. In Fig. 4, we have investigated the effect of different  $\Delta$  values on the temperature-dependent curves of entropy and Josephson current for different  $t_{12}$ . In Figs. 4(a) and 4(c), we first consider the case where the interdot coupling coefficient is relatively small, i.e.,  $t_{12} = 0.01$ . The solid black line in Fig. 4(a) shows how the entropy of the system changes with temperature when the electrode is in the normal metal state  $\Delta = 0$ . It clearly shows that  $S_{QD}$ 's magnitude reduces in the stepwise manner, following the decrease of temperature. And then, the corresponding characteristic phase transition temperatures can be defined. When the QD system is in the FOR,  $S_{QD} = 2 \ln 4$ . With the temperature decreasing, the system reaches the local magnetic-moment regime. Herein, the empty states  $|0\rangle$  and double-occupied states  $|\uparrow\downarrow\rangle$  are both suppressed, while the two single-occupied states  $|\uparrow\rangle$  and  $|\downarrow\rangle$  appear with equal probability. As a result, the entropy is halved with  $S_{QD} = \ln 4 = 2 \ln 2$ . At the step transition point between two entropy values, we can define  $T_U = (T_{S=2 \ln 4} + T_{S=\ln 4})/2$ . As the temperature further reduces, the QD system enters ferromagnetic frozen region (FFR) with total spin  $S = 1$ , due to the RKKY interaction. Consequently, the entropy further decreases to  $S_{QD} = \ln(2S + 1) = \ln 3$ . We can define a characteristic transition temperature  $T_F = (T_{S=\ln 4} + T_{S=\ln 3})/2$ . As the temperature continues to drop, the total spin of the electrons in the DQDs is screened by the free electrons in the electrode, the total spin of the QDs reduces from  $S = 1$  to  $\frac{1}{2}$ , the system

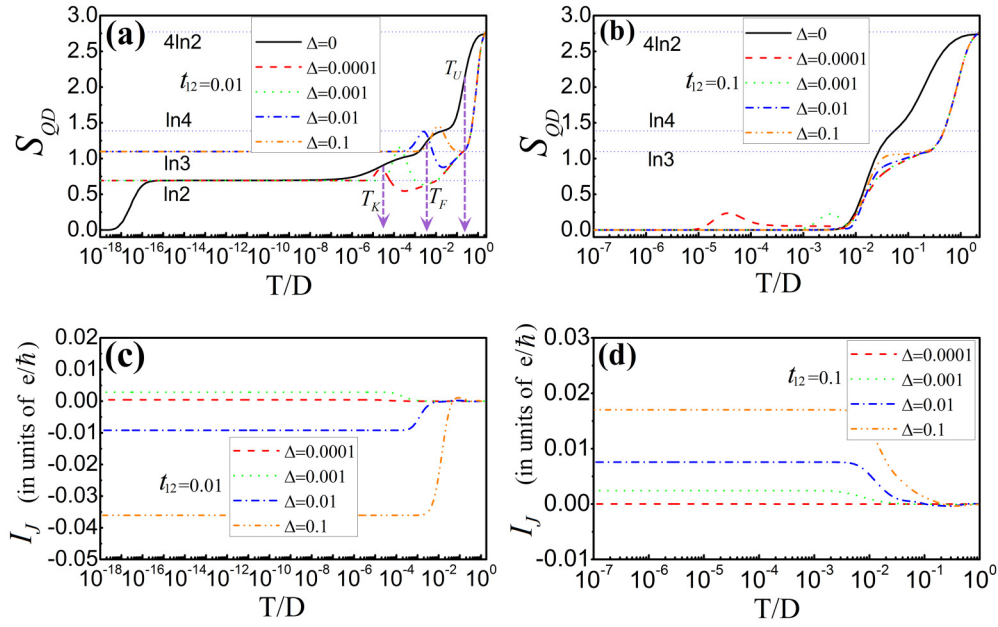


FIG. 4. (a), (b) The entropy of the system as a function of temperature for various  $\Delta$  in the case of  $t_{12} = 0.01$  and  $= 0.1$ , respectively. (c), (d) The Josephson current as a function of temperature for different  $\Delta$  in the cases of  $t_{12} = 0.01$  and  $= 0.1$ , respectively. We take  $\varepsilon_j = -U/2$ , with other system parameters remaining the same as in Fig. 2.

enters strong coupling region, and the entropy decreases to  $S_{\text{QD}} = \ln(2S + 1) = \ln 2$ . The total spin of QDs is partially screened, i.e., is an underscreening Kondo state composed of a Fermi liquid with a residual spin  $\frac{1}{2}$ . Accordingly, we can define a characteristic transition temperature  $T_K = (T_{S=\ln 3} + T_{S=\ln 2})/2$ , which corresponds to the Kondo temperature of the system. When the temperature further decreases, the interdot antiferromagnetic correlation mechanism gradually becomes the dominant factor among the several competing correlation mechanisms in the system. This results in the total spin of the system being 0 and the entropy decreasing to 0. Correspondingly, the characteristic temperature can be defined as  $T_{\text{AF}} = (T_{S=\ln 2} + T_{S=0})/2$ . When  $\Delta$  gradually increases, the entropy values of the QD stay on the different platforms, which means that the system reaches different fixed points at low temperatures. Specifically, when  $\Delta = 0.0001$  and  $0.001$ , the entropy flow curve of the QDs no longer reaches 0 at low temperature, but remains constant after reaching a platform with the value of  $\ln 2$ . However, with the  $\Delta$  further increasing ( $\Delta = 0.01$  and  $0.1$ ), the entropy remains constant, namely,  $S_{\text{QD}} = \ln 3$ , which means that the total spin  $S$  is unscreened at low temperatures.

These interesting phenomena stem from the competition among the characteristic energy scales of several electron correlation effects in this system. When  $t_{12}$  is relatively small,  $J_{\text{RKKY}} \gg J_{\text{AF}}$ , which of the two fixed points is reached by entropy flow depends on the competition between  $\Delta$  and  $T_K$ . When  $\Delta \ll T_K$ , the stable Kondo fixed point entropy of the DQD is  $\ln 2$ , indicating that the total spin  $S$  is underscreened. The Josephson junction is in the  $0$ -phase regime, and the current amplitude is greatly suppressed, as shown in Fig. 4(c). However, with further increase of  $\Delta$ , it will have the capability to suppress the Kondo effect when  $\Delta \gg T_K$ , and the entropy  $S_{\text{QD}} = \ln 3$ , indicating that the total spin  $S$  is unscreened. Therefore, the current turns negative and its

absolute value significantly increases, indicating the presence of a  $0-\pi$  junction phase transition phenomenon.

When the interdot coupling coefficient is larger, i.e.,  $t_{12} = 0.1$ , then  $J_{\text{AF}} \gg J_{\text{RKKY}}$ . As the temperature decreases, the entropy  $S_{\text{QD}}$  decreases to 0 for all values of  $\Delta$ , as shown in Fig. 4(b). However, there are several differences between the curves for different  $\Delta$ . First, when  $\Delta = 0$ , the DQD is in the antiferromagnetic singlet because the  $J_{\text{AF}}$  becomes the dominant mechanism among the several competing energies. The RKKY mechanism is severely suppressed at this time. Therefore, the entropy of the system is directly reduced from  $\ln 4$  to 0, and the platform with entropy equal to  $\ln 3$  disappears. However, when  $\Delta \neq 0$ , the entropy curves experience an obvious plateau  $S_{\text{QD}} = \ln 3$  in the process of temperature reduction. It means that the temperature of the system is in  $T_F > T$ , and  $T_F$  is the dominant characteristic temperature. And then we can see that at even lower temperatures,  $S_{\text{QD}}$  goes to 0. This indicates that although the presence of the  $\Delta$  can facilitate the formation of RKKY,  $T_{\text{AF}}$  is the dominant characteristic temperature when the temperature is sufficiently low. Second, all curves in Fig. 4(b) tend to have zero entropy at almost the same temperature value. This is because when  $t_{12}$  is large, the antiferromagnetic interaction becomes the dominant mechanism, and the magnitude of  $\Delta$  has little influence on it. Therefore, with the increase of  $\Delta$ , the Josephson current of the system continuously increases from small to large and maintains the positive current. There is no  $0-\pi$  transition phenomenon characterized by the reverse direction of Josephson current, as shown in Fig. 4(d).

## B. Delocalized control of YSR state and magnetic order of DQD

In Figs. 5(a) and 5(b), we plotted the Josephson current and the interdot spin correlation  $\langle S_1 S_2 \rangle$  as functions of the superconducting phase difference  $\varphi$ . It can be seen from

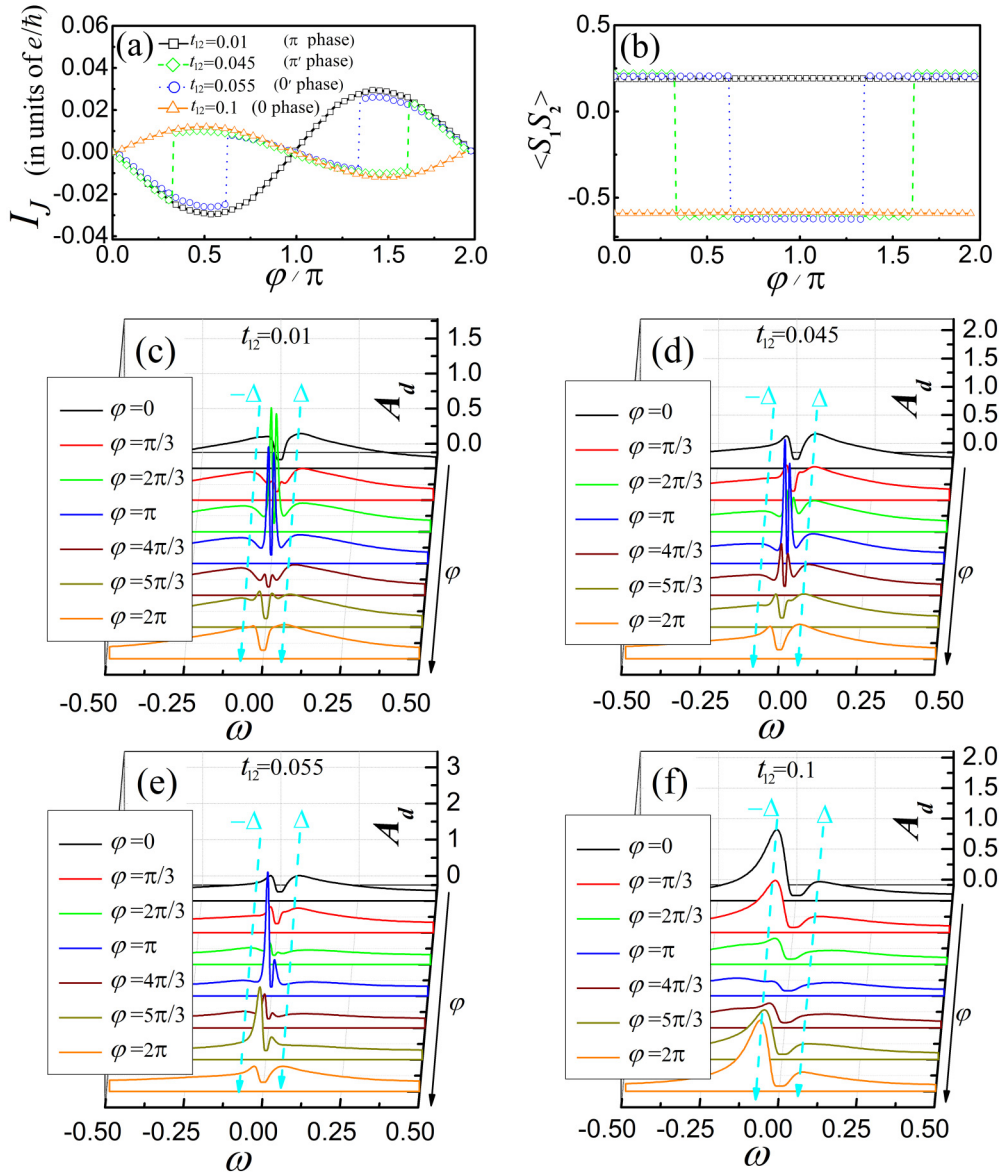


FIG. 5. (a) The Josephson current as functions of  $\varphi$  with various  $t_{12}$ . (b) Spin correlation  $\langle S_1 S_2 \rangle$  as functions of  $\varphi$  with various  $t_{12}$ . (c)–(f) The evolution of spectral function curve of the QDs with increasing  $\varphi$  for various  $t_{12}$ . Other system parameters are set as  $\varepsilon_j = -U/2$ .

Fig. 5(a) that the system gradually changes from  $\pi$  junction to  $0$  junction when  $t_{12}$  increases. At the same time, the spin correlation  $\langle S_1 S_2 \rangle$  shows a gradual transition from ferromagnetic to antiferromagnetic, as shown in Fig. 5(b). Interestingly, in the two cases of  $t_{12} = 0.045$  and  $t_{12} = 0.055$ , the system is in the transition phase  $\pi'$  and  $0'$ , and the current curves present the kinklike feature. Additionally, when  $t_{12} = 0.045$  (or  $t_{12} = 0.055$ ), by adjusting the phase difference within the range of  $0.4\pi \leq \varphi \leq 1.6\pi$  (or  $0.6\pi \leq \varphi \leq 1.4\pi$ ), the value of  $\langle S_1 S_2 \rangle$  changes from positive to negative, with a magnitude of approximately  $-0.6$ . It means that there will be a transition from ferromagnetic to antiferromagnetic between the single-occupied electrons located in the two QDs. More importantly, this triplet-to-singlet transition is caused by delocalized adjustment of the external electrode phase difference. In comparison to the manipulation of  $0$ - $\pi$  transition through superconducting phase difference here, Ryzanov *et al.*

reported a thermally induced  $0$ - $\pi$  phase transition mechanism [64,65]. In S/F/S Josephson junctions, the variation in temperature can lead to a change in the coherence length due to the relatively weak intermediate ferromagnetic layer, thereby enabling the phase of the superconducting order parameter in the ferromagnet to switch from  $0$  to  $\pi$ . Therefore, it is believed that future theoretical and experimental studies may reveal more sophisticated means of modulating Josephson phase transitions.

In order to investigate the evolution of the YSR state in the  $\pi$ - $0$  junction transition, in Figs. 5(c)–5(f), the spectral functions of the QDs are presented with increasing  $\varphi$  under various values of  $t_{12}$ . When  $t_{12} = 0.01$ , as  $\varphi$  increases from  $0$  to  $\pi$ , the YSR state peaks gradually emerge within the gap, and the heights of peaks increase. The position of the peak exhibits a symmetry about  $\omega = 0$  and gradually approaches the symmetry point, indicating that the YSR states will undergo

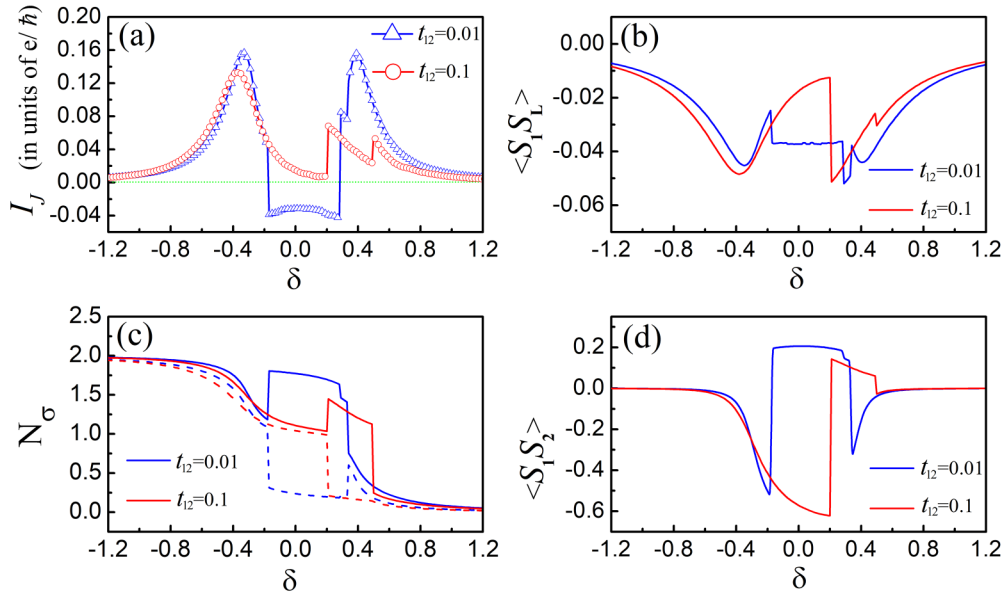


FIG. 6. (a), (c) The Josephson current and the number of electrons in DQD as a function of the energy level  $\delta$ , respectively. (b), (d) The spin correlation functions  $\langle S_1 S_L \rangle$  and  $\langle S_1 S_2 \rangle$  as a function of the energy level  $\delta$ , respectively. Other system parameters are set as  $\varphi = \pi/2$ .

zero-energy crossover. Subsequently, as  $\varphi$  increases from  $\pi$  to  $2\pi$ , the height and position of YSR peaks exhibits an opposite trend compared to the previous situation, and gradually returning to the shape of  $\varphi = 0$ . With  $t_{12}$  increasing from 0.045 to 0.1, as depicted in Figs. 5(d)–5(f), it can be observed that not only does the YSR peak gradually transform from symmetric about  $\omega = 0$  to asymmetric, but the parameter range with YSR peaks also gradually diminishes and finally disappears completely in Fig. 5(f). This outcome is attributed to the gradual formation of bonding and antibonding states of electrons in QDs under the influence of  $t_{12}$  [36,66]. As discussed above, the magnetic order and current direction in a DQD Josephson junction can be adjusted by system parameters, such as  $t_{12}$ . Moreover, when  $t_{12}$  is fixed, we can manipulate the magnetic order and YSR state in a “remote” manner by adjusting the superconducting phase difference  $\varphi$ . This provides us with an approach to delocalized control of YSR states, which is different from STM probe technology [38].

The QD level is an important tunable parameter in our model. Next, we will further determine the range of QD level  $\varepsilon_j$ , in which one can effectively adjust the magnetic order mentioned above. In Figs. 6(a)–6(d), the curves of Josephson current, the  $\sigma$  component of total number of electrons in the QD molecule, and spin correlation functions are plotted as functions of the QD energy level for various  $t_{12}$ . The curves of  $\langle S_1 S_L \rangle$  depicted here are analogous to  $\langle S_1 S_2 \rangle$  in Fig. 2, and it represents the spin correlation between QD-1 and the left lead. Therefore, its thermodynamic expectation value can be obtained by the formula [67]  $\langle S_1 S_L \rangle = \langle S_1 \cdot S_L \rangle$ . Here,  $S_1 = \frac{1}{2} \sum_{\sigma, \sigma'} d_{1\sigma}^\dagger \hat{\sigma}_{\sigma, \sigma'} d_{1\sigma'}$  and  $S_L = \frac{1}{2} \sum_{j, k, k', \sigma, \sigma'} a_{j, k, \sigma}^\dagger \hat{\sigma}_{\sigma, \sigma'} a_{j, k', \sigma'}$ , where  $\hat{\sigma}$  is a vector of Pauli matrices. Additionally, the value of  $N_\sigma$  can be obtained using the following expression:

$$N_\sigma = \sum_{j=1}^2 \langle n_{j\sigma} \rangle, \quad (12)$$

where  $\langle n_{j\sigma} \rangle$  represents the  $\sigma$  component of particle number in the QD- $j$ . It can be obtained using standard Green’s function techniques, as it is related to the lesser Green function:

$$\langle n_{j\sigma} \rangle = -i \int \frac{d\omega}{2\pi} G_{j\sigma}^<(\omega). \quad (13)$$

Here, we set  $\delta = \varepsilon_j + U/2$ . In Fig. 6(a), one can notice that when  $t_{12} = 0.01$ , the shape of the current curve is almost the same as that in the  $t_{12} = 0$  case. When adjusting the QD energy levels within the range of  $-0.2 \leq \delta \leq 0.3$ , the Josephson junction enters  $\pi$  phase, and the Josephson current  $I$  is negative; correspondingly, the values of  $\langle S_1 S_L \rangle$  and  $\langle S_1 S_2 \rangle$  are  $-0.04$  and  $0.2$ , respectively, as shown in Figs. 6(b) and 6(d). The results indicates that there is very weak antiferromagnetic correlation between QDs and electrodes, while there is ferromagnetic arrangement between the electrons in the QDs. This can be explained as follows: within this range of  $\delta$ , the Kondo effect is suppressed by the superconducting correlation effect, and the local magnetic moment of the QDs cannot be screened by the Kondo cloud. So, the curves of  $N_\sigma$  (blue solid line) and  $N_{\bar{\sigma}}$  (blue dashed line) show a significant difference, as shown in Fig. 6(c).

Now, let us shift our attention beyond this range, at  $\delta \approx \pm 0.4$ , where the Josephson current curve in Fig. 6(a) has two peaks. This is because the Kondo exchange coefficient between the QD and the external electrode can be expressed as [59]

$$J_K = 2V_{K_F}^2 \left( \frac{1}{|\delta - U/2|} + \frac{1}{|\delta + U/2|} \right). \quad (14)$$

When the QD energy level approaches  $\delta = \pm U/2$ , Kondo temperature  $T_K$  increases sharply. Therefore, the curve of  $\langle S_1 S_L \rangle$  in Fig. 6(b) has two small negative peaks and the value of  $\langle S_1 S_2 \rangle$  in Fig. 6(d) is suppressed at the same time. The curves of  $N_\sigma$  and  $N_{\bar{\sigma}}$  in Fig. 6(c) tend to coincide, implying that the local magnetic moment disappears.



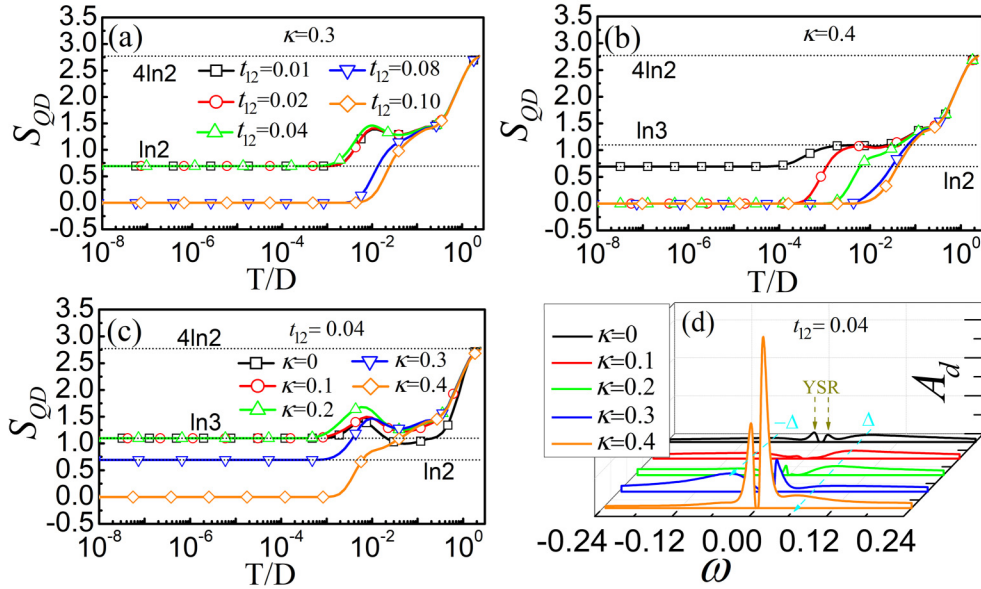


FIG. 7. (a), (b) Temperature dependence of the entropy with various  $t_{12}$  in the case of  $\kappa = 0.3$  and  $\kappa = 0.4$ , respectively. (c) Temperature dependence of the entropy with various  $\kappa$  in the case of  $t_{12} = 0.04$ . (d) Spectral function curves of the QD corresponding to (c). Other system parameters remaining are taken to be  $\varepsilon_j = -U/2$ ,  $\varphi = \pi/2$ .

In contrast, when  $t_{12}$  increases to 0.1, the current curve changes in two aspects: on the one hand, the  $\pi$ -phase region around  $\delta = 0$  disappears; on the other hand, the shape of the curve is no longer symmetrical. For the former change, the underlying physical mechanism is not  $T_K \gg \Delta$ , instead, the two single-occupied electrons in the QD form strong anti-ferromagnetic correlation, resulting in the formation of local spin singlet. However, the latter one is due to the presence of bonding and antibonding states, which directly leads to the loss of electron-hole symmetry in both current curves and spectral function's YSR states.

### C. SU(4) Kondo effect and orbital YSR states

For real DQD systems, when the distance between two dots is close, the interdot Coulomb interaction  $U_{12}$  may have a significant modulating effect on the  $0-\pi$  phase transition and YSR states in the system. Additionally, it is challenging to experimentally fabricate two QDs with precisely identical properties, especially ensuring that both QDs have the same onsite energy  $\varepsilon_j$ . Therefore, we introduce new parameters  $\kappa$  and  $U_{12}$  into the Hamiltonian  $H_{\text{DQD}}$  in Eq. (2), representing the onsite energy splitting and interdot Coulomb interaction, respectively. Thus, the new form of the QDs Hamiltonian is expressed as follows:

$$H_{\text{DQD}} = \sum_{\sigma, j=1}^2 \xi_j d_{j\sigma}^\dagger d_{j\sigma} + \sum_{j=1}^2 U_j n_{j\uparrow} n_{j\downarrow} + U_{12} n_1 n_2 + \sum_{\sigma} (t_{12} d_{1\sigma}^\dagger d_{2\sigma} + \text{H.c.}), \quad (15)$$

where  $\xi_1 = (\varepsilon_1 + U_1/2) + \kappa$  and  $\xi_2 = (\varepsilon_2 + U_2/2) - \kappa$ . We assume that the actual energy levels of two QDs are  $\xi_j = \pm\kappa$ , which means that the energy levels of the two QDs respect to their respective electron-hole symmetric points  $\varepsilon_j = -U_j/2$

are shifted by  $\pm\kappa$ . In Figs. 7(a)–7(c), we depict the entropy of QDs as a function of temperature under various values of  $\kappa$  and  $t_{12}$  when  $U_{12} = 0$ . First, by comparing Fig. 7(a) with Fig. 2(a), it is evident that the introduction of level splitting  $\kappa$  can enhance the Kondo exchange coefficient  $J_K$  when  $U_{12} = 0$ . This results in the value of entropy flow at the low-temperature fixed point decreasing from  $\ln 3$  in Fig. 2(a) to  $\ln 2$  here when  $t_{12} \leq 0.04$ . In other words, the total magnetic moment of the parallel DQDs transitions from unscreened state to underscreened state. However, when  $t_{12} > 0.04$ , as shown in Fig. 2(a), the QD molecule still forms an anti-ferromagnetic singlet  $S = 0$  due to the gradual dominance of anti-ferromagnetic correlation energy. In Fig. 7(b), as  $\kappa$  increases to 0.4, compared to Fig. 7(a), it is observed that at smaller values of  $t_{12}$ , specifically when  $t_{12} = 0.02$ , the magnetic order of the QD molecule can enter the anti-ferromagnetic phase. Referring to Eq. (A6) in the Appendix, it is noted that when  $\kappa$  is present, it should be rewritten as follows:

$$J_{\text{AF}} \approx \frac{4t_{12}^2 U}{U^2 - 4\kappa^2}. \quad (16)$$

So, within a certain range, increasing  $\kappa$  can simultaneously increase both  $J_K$  and  $J_{\text{AF}}$ . However, the higher the value of  $t_{12}$ , the faster  $J_{\text{AF}}$  will increase. This is manifested that for different  $t_{12}$  values, the system's entropy flow corresponds to different fixed points. In Fig. 7(c), we set  $t_{12} = 0.04$  and conducted a detailed investigation into the influence of different strengths of  $\kappa$  on the system's entropy flow, and plotted the corresponding spectral function curves in Fig. 7(d). It is found that even if  $t_{12}$  is fixed, as  $\kappa$  gradually increases, due to the gradual increase in the Kondo temperature, the fixed points of the entropy flow curve undergo some discontinuous transitions from  $\ln 3 \rightarrow \ln 2 \rightarrow 0$ . The system also transitions from the  $S = 1$  triplet state to the  $S = \frac{1}{2}$  doublet state, and finally

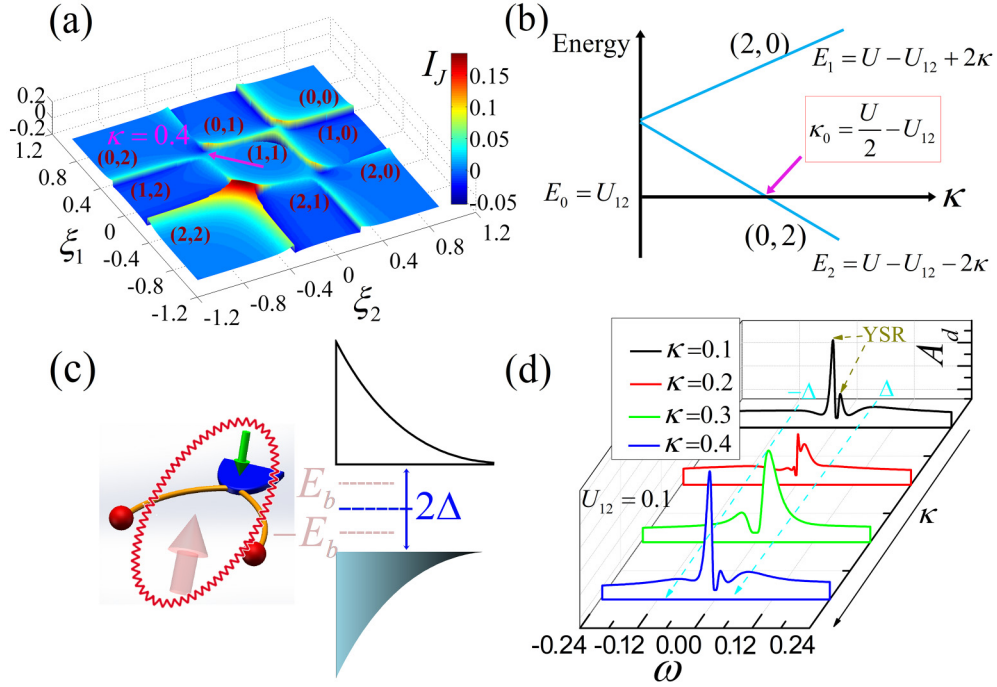


FIG. 8. (a) The Josephson current as a function of the QD energy level  $\xi_{1(2)}$  with  $t_{12} = 0.04$ . (b) Schematic diagram of the energy levels vary with  $\kappa$  for the isolated DQD system. (c) Schematic diagram of orbital YSR states arise from pseudospins and quasiparticles outside the superconducting gap. (d) The evolution of spectral function curve of the QDs with increasing  $\kappa$  for  $U_{12} = 0.1$ . Other parameters are consistent with those in Fig. 2.

to the  $S = 0$  antiferromagnetic singlet state. Correspondingly, the two symmetric YSR peaks within the superconducting gap in Fig. 7(d) are gradually suppressed. Interestingly, at  $\kappa = 0.4$ , two robust asymmetric new peaks reappear within the gap.

To investigate the physical mechanism behind the new spectral peaks emerging within the superconducting gap, we plotted a two-dimensional diagram of the Josephson current as a function of the QD levels  $\xi_1$  and  $\xi_2$  under  $t_{12} = 0.04$ , as shown in Fig. 8(a). It can be observed that with the variation of the QD levels, there are a series of  $\pi$ -phase regions (dark blue regions) divided by the current peaks. This is very similar to the charge stability diagram divided by Coulomb peaks when normal electrodes are connected [41]. In each hexagonal region, the numbers of electrons ( $n, m$ ) have been marked in the diagram. Along this diagonal line  $\xi_1 = -\xi_2$ , there are three regions with different electron filling configurations in the diagram:  $(0,2)$ ,  $(1,1)$ , and  $(2,0)$ , corresponding to six different electron states.

As  $\kappa$  increases, the spin singlet  $|S\rangle = \frac{1}{\sqrt{2}}[|\downarrow_1\uparrow_2\rangle - |\uparrow_1\downarrow_2\rangle]$  and the spin triplet  $|T_0\rangle = \frac{1}{\sqrt{2}}[|\downarrow_1\uparrow_2\rangle + |\uparrow_1\downarrow_2\rangle]$ ,  $|T_-\rangle = |\downarrow_1\downarrow_2\rangle$ ,  $|T_+\rangle = |\uparrow_1\uparrow_2\rangle$  remain fourfold degenerate, with energy eigenvalues  $E_0 = U_{12}$ . But, the other two states  $|D_1\rangle = |\uparrow_1\downarrow_1\rangle$ ,  $|D_2\rangle = |\uparrow_2\downarrow_2\rangle$  exhibit level splitting as  $\kappa$  increases, with energy levels  $E_{1(2)} = U - U_{12} \pm 2\kappa$ . When  $\kappa_0 = U/2 - U_{12}$ , as indicated by the light red arrows in Figs. 8(a) and 8(b), a fivefold degeneracy emerges within the DQD molecule, namely, the four spin states associated with the  $(1,1)$  occupancy and one orbital state of  $(0,2)$  occupancy form a fivefold degeneracy, and the pseudospin-flip events for  $(1,1) \leftrightarrow (0,2)$  can lead to

a Kondo correlation effect. When the spin and orbital degrees of freedom satisfy the  $SU(4)$  symmetry, their strong mixing yields a  $SU(4)$  Kondo effect. At this time, the pseudospin states in the DQD molecule can also form YSR states with quasiparticles outside the superconducting gap, similar to genuine localized spins, which are called the *orbital YSR states*, as shown in Fig. 8(c). When there is interdot Coulomb interaction between the DQDs, the degeneracy point  $\kappa_0$  will decrease with the increase of  $U_{12}$ . In Fig. 8(d), it can be observed that when  $U_{12} = 0.1$ , as  $\kappa$  increases from 0.1 to 0.4, the spin YSR states are gradually suppressed. However, when  $\kappa = 0.3$ , a pair of asymmetric orbital YSR peaks appears. When  $\kappa$  increases to 0.4, the spin YSR peaks gradually recover.

To further clarify that the two types of YSR peaks originate from different physical mechanisms, we apply an external magnetic field to the QDs, which can suppress the spin Kondo effect but does not affect the orbital Kondo effect. We expect that the orbital YSR peaks will remain fixed at the original position  $\kappa_0 = U/2 - U_{12}$ . In Figs. 9(a) and 9(b), it can be observed that along the diagonal line where  $\xi_1 = \xi_2$ , i.e.,  $\kappa = 0$ , the Josephson current peaks originally presented in Fig. 8(a) have disappeared due to the effect of the magnetic field. On the other hand, due to the Zeeman splitting of the triplet energy levels, the energy level of the  $|T_+\rangle$  state becomes  $E_+ = U_{12} - 2E_Z$  (where  $E_Z$  represents the Zeeman energy), and it undergoes singlet-triplet degeneracy with the energy level  $E_2 = U - U_{12} - 2\kappa$  of the  $|D_2\rangle$  state at  $\kappa_0 = U/2 - U_{12} + E_Z$ . Therefore, a pair of new current peaks emerges at  $\kappa = 0.6$ , as indicated by the light red arrow in Fig. 9(a). In Fig. 9(c), it can be observed that at  $\varepsilon_1 = \varepsilon_2 = -U/2$ , i.e.,  $\kappa = 0$ , the

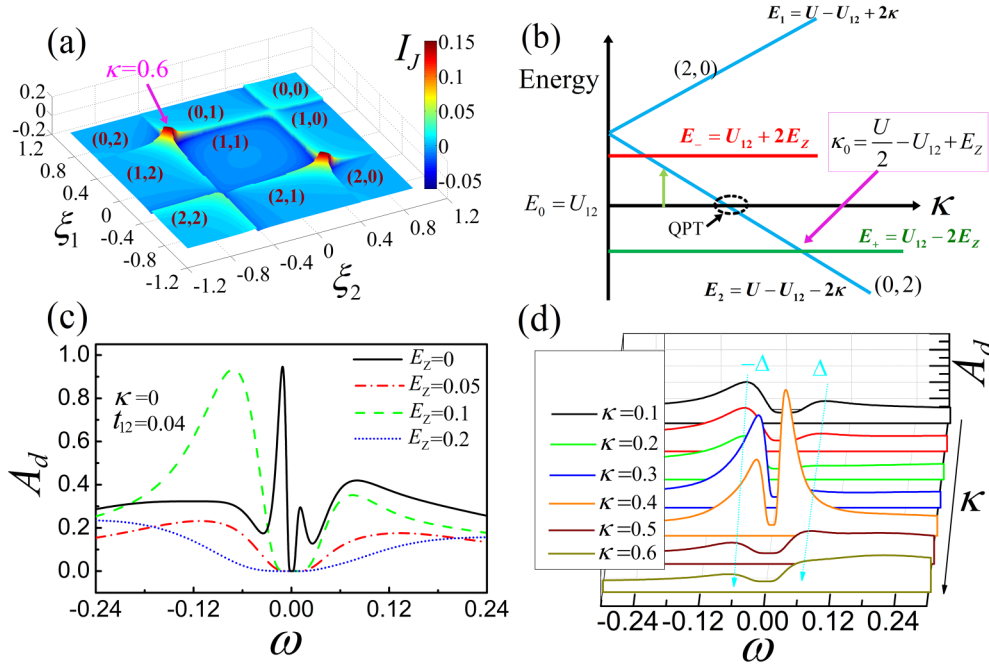


FIG. 9. (a) Josephson current as a function of the QD level  $\xi_{1(2)}$  when Zeeman energy  $E_Z = 0.2$ . (b) Schematic diagram of the energy levels of an isolated DQD system as functions of  $\kappa$ . (c) Spectral function curves of the QD with various  $E_Z$  in the case of  $\kappa = 0$  and  $t_{12} = 0.04$ . (d) The evolution of spectral function curve of the QDs with increasing  $\kappa$  for  $U_{12} = 0$ . Other parameters are the same as those in Fig. 8.

spin YSR peaks originally existing in the superconducting gap gradually disappears with the increase of Zeeman energy  $E_Z$ . However, in Fig. 9(d), as  $\kappa$  is adjusted to the quantum phase transition (QPT) point at  $\kappa = 0.4$ , the  $|D_2\rangle$  state degenerates with the  $|S\rangle$  and  $|T_0\rangle$  states, which also have a total spin  $S = 0$ . As a result, the orbital YSR peaks still emerge as expected.

Recently, Xia *et al.* investigated the YSR states of the molecular magnet  $\text{Tb}_2\text{Pc}_3$  on a superconducting  $\text{Pb}(111)$  substrate [39]. The experimental results reveal the presence of two distinct YSR states with different physical origins in the system. Moreover, as the tunneling current of the STM tip varies, these two pairs of YSR resonance peaks exhibit significantly different behaviors in terms of their energy-level positions and intensities. The energy positions of a pair of YSR peaks on the inner side strongly depend on the tip height of STM, while another pair of peaks on the outer side only shows slight movement. Theoretical calculations reveal that these two sets of YSR states originate from ligand spin and higher charge fluctuations in unoccupied molecular orbitals, coexisting within a single molecule. Based on these experimental reports, we believe that the theoretical research results of this paper can provide unique insights into the different mechanisms of YSR states in experiments.

#### IV. SUMMARY

In summary, by using the NRG technique, we have theoretically investigated the  $0-\pi$  phase transition and the YSR state in a parallel-coupled DQD Josephson junction. The calculation results show that there are many kinds of competing and cooperating electron correlation effects in this model. By adjusting the interdot coupling coefficient  $t_{12}$ , the relative magnitude of the  $J_{\text{RKKY}}$  and  $J_{\text{AF}}$  can be changed, and the

$0-\pi$  phase transition behavior of Josephson junction can be affected.

First of all, when the value of  $t_{12}$  is relatively small,  $J_{\text{RKKY}} \gg J_{\text{AF}}$ , the magnetic order of the QD molecular exhibits ferromagnetic behavior. At low temperature, the entropy of QDs is manifested as the residual entropy of  $\ln 2$  or  $\ln 3$ . It depends on the competition between the characteristic energy scales  $\Delta$  of superconducting pairing potential and the Kondo temperature  $T_K$  in the system. When  $T_K \gg \Delta$ , the entropy of stable Kondo fixed point at low temperatures is  $\ln 2$ , indicating that the superconducting electrodes are under-screened with respect to the QD molecule. The Josephson junction is in the  $0$ -phase regime, and the current amplitude is greatly suppressed. Conversely, when  $T_K \ll \Delta$ , the low-temperature fixed point of the system corresponds to an entropy of  $\ln 3$ , indicating that the superconducting electrodes are in completely unscreened states with respect to the QD molecule. The Josephson junction is in the  $\pi$ -phase regime, and the critical Josephson current  $I_C$  amplitude increases with increasing  $\Delta$ .

Second, when the value of  $t_{12}$  is relatively large,  $J_{\text{RKKY}} \ll J_{\text{AF}}$ , the magnetic order of the QD molecule presents antiferromagnetic arrangement. In this case, the RKKY interaction between the electrons is severely suppressed, and the entropy of the system eventually approaches 0 when the temperatures are sufficiently low. With the increase of  $\Delta$ , the Josephson current of the system gradually increases and remains consistently positive, and there is no  $0-\pi$  transition phenomenon in the Josephson junction.

Third, we find that the transition between singlet and triplet states can be controlled by adjusting the phase difference  $\varphi$  of the superconducting electrode even if  $t_{12}$  is fixed. We can use it to regulate the magnetic order and YSR states of

the DQDs in a delocalized manner. This physical mechanism can be applied to construct and regulate the superconducting nanodevices and quantum bits.

Finally, by adjusting the QD energy level  $\xi_{1(2)} = \pm\kappa$ , when the level detuning value  $\kappa$  is at the degeneracy point, the spin and orbital degrees of freedom satisfy the SU(4) symmetry. Their strong mixing yields an SU(4) Kondo effect. The spectral function of QDs will show YSR peaks in the superconducting gap caused by different Kondo correlations. By applying an external magnetic field, we have confirmed the underlying physical mechanisms behind the emergence of this orbital Kondo YSR peak.

### ACKNOWLEDGMENTS

Special thanks are extended to T.-H. Yi for his helpful discussions and several thorough readings on the manuscript. This work was financially supported by the Liaoning Revitalization Talents Program (Grant No. XLYC1907033), the Natural Science Foundation of Liaoning province (Grant No. 2023-MS-072). Our numerical results are obtained via ‘‘NRG Ljubljana,’’ open source numerical renormalization group code.

### APPENDIX: DERIVE EXCHANGE COEFFICIENT $J_{AF}$ IN THE DQD-SYSTEM USING THE PERTURBATION THEORY

Considering an isolated DQD system, the QDs are connected by the interdot coupling coefficient  $t_{12}$ , and the Hamiltonian can be expressed as

$$H_{\text{DQD}} = \sum_{\sigma,j=1}^2 \varepsilon_j d_{j\sigma}^\dagger d_{j\sigma} + \sum_{j=1}^2 U_j n_{j\uparrow} n_{j\downarrow} + U_{12} n_1 n_2 + \sum_{\sigma} (t_{12} d_{1\sigma}^\dagger d_{2\sigma} + \text{H.c.}), \quad (\text{A1})$$

where  $U_{12}$  and  $U_j$  represent the interdot and intradot Coulomb interactions in the DQD system, respectively. To investigate the antiferromagnetic exchange coefficient  $J_{AF}$  between QDs, we consider the charge occupation configurations in the coupled DQDs: (1,1), (0,2), and (2,0). These correspond to six different basis vectors:

$$|1\rangle = |S\rangle = \frac{1}{\sqrt{2}} [|\downarrow_1\uparrow_2\rangle - |\uparrow_1\downarrow_2\rangle], \quad (\text{A2a})$$

$$|2\rangle = |T_0\rangle = \frac{1}{\sqrt{2}} [|\downarrow_1\uparrow_2\rangle + |\uparrow_1\downarrow_2\rangle], \quad (\text{A2b})$$

$$|3\rangle = |T_-\rangle = |\downarrow_1\downarrow_2\rangle, \quad (\text{A2c})$$

$$|4\rangle = |T_+\rangle = |\uparrow_1\uparrow_2\rangle, \quad (\text{A2d})$$

$$|5\rangle = |D_1\rangle = |\uparrow_1\downarrow_1\rangle, \quad (\text{A2e})$$

$$|6\rangle = |D_2\rangle = |\uparrow_2\downarrow_2\rangle. \quad (\text{A2f})$$

Exact diagonalization of the Hamiltonian in Eq. (A1) in the basis of six states above enables us to obtain the effective Hamiltonian matrix

$$\hat{H}_D^{\text{eff}} = \hat{E}_0 + \begin{pmatrix} 0 & 0 & 0 & 0 & -\sqrt{2}t_{12} & -\sqrt{2}t_{12} \\ 0 & 0 & 0 & 0 & 0 & 0 \\ 0 & 0 & 0 & 0 & 0 & 0 \\ 0 & 0 & 0 & 0 & 0 & 0 \\ -\sqrt{2}t_{12} & 0 & 0 & 0 & E_1 & 0 \\ -\sqrt{2}t_{12} & 0 & 0 & 0 & 0 & E_2 \end{pmatrix}. \quad (\text{A3})$$

Here  $\hat{E}_0 = (U_{12} + \varepsilon_1 + \varepsilon_2)\hat{I}$ ,  $E_1 = U_1 - U_{12} + \tilde{\varepsilon}$ ,  $E_2 = U_2 - U_{12} - \tilde{\varepsilon}$ ,  $\tilde{\varepsilon} = \varepsilon_1 - \varepsilon_2$ , and  $\hat{I}$  is the unit matrix.

In considering the relative magnitudes of parameters in typical coupled QDs, where  $U_j \gg t_{12}$  and  $U_j \gg U_{12}$ , we can utilize Rayleigh-Schrödinger perturbation theory to calculate second-order corrections in  $t_{12}$  to the energy of a state [60]. Up to the second order in  $t_{12}$ , the energy correction for state  $|n\rangle$  of the DQD is

$$E_n^{(2)} = \sum_{m \neq n}^m \frac{\langle n|H_c|m\rangle \langle m|H_c|n\rangle}{E_n - E_m}. \quad (\text{A4})$$

We consider the second-order energy corrections between the singlet state  $|S\rangle = \frac{1}{\sqrt{2}} [|\downarrow_1\uparrow_2\rangle - |\uparrow_1\downarrow_2\rangle]$  and the triplet state  $|T\rangle$ , denoted by  $E_S^{(2)}$  and  $E_T^{(2)}$ , respectively. We define the interdot antiferromagnetic exchange coefficient as  $J_{AF} = E_S^{(2)} - E_T^{(2)}$ . Thus, it can be expressed as follows:

$$\begin{aligned} J_{AF} &= E_S^{(2)} - (E_{T_0}^{(2)} + E_{T_+}^{(2)} + E_{T_-}^{(2)}) \\ &= 2t_{12}^2 \left[ \frac{1}{U_1 - U_{12} + (\varepsilon_1 - \varepsilon_2)} + \frac{1}{U_2 - U_{12} - (\varepsilon_1 - \varepsilon_2)} \right] \\ &= 2t_{12}^2 \left[ \frac{1}{U_1 - U_{12} + \tilde{\varepsilon}} + \frac{1}{U_2 - U_{12} - \tilde{\varepsilon}} \right], \end{aligned} \quad (\text{A5})$$

where  $\tilde{\varepsilon} = \varepsilon_1 - \varepsilon_2$ . If  $U_{12} \ll U_j$  and the parameters of the two QDs are completely symmetric, namely,  $U_1 = U_2 = U$  and  $\varepsilon_1 = \varepsilon_2$ . Then,

$$J_{AF} \approx \frac{4t_{12}^2}{U}. \quad (\text{A6})$$

- [1] E. B. Foxman, P. L. McEuen, U. Meirav, Ned S. Wingreen, Y. Meir, Paul A. Belk, N. R. Belk, M. A. Kastner, and S. J. Wind, Effects of quantum levels on transport through a Coulomb island, *Phys. Rev. B* **47**, 10020(R) (1993).  
 [2] W. G. Van der Wiel, S. De Franceschi, T. Fijisawa, J. M. Elzerman, S. Tarucha, and L. P. Kouwenhoven, The Kondo effect in the unitary limit, *Science* **289**, 2105 (2000).

- [3] J. P. Cleuziou, W. Wernsdorfer, V. Bouchiat, T. Ondarcuhu, and M. Monthieux, Carbon nanotube superconducting quantum interference device, *Nat. Nanotechnol.* **1**, 53 (2006).  
 [4] R. Potok, I. Rau, H. Shtrikman *et al.*, Observation of the two-channel Kondo effect, *Nature (London)* **446**, 167 (2007).  
 [5] H. B. Heersche, Z. de Groot, J. A. Folk, L. P. Kouwenhoven, H. S. J. van der Zant, A. A. Houck, J. Labaziewicz, and I. L.

- Chuang, Kondo effect in the presence of magnetic impurities, *Phys. Rev. Lett.* **96**, 017205 (2006).
- [6] Y. Nagaoka, Self-consistent treatment of Kondo's effect in dilute alloys, *Phys. Rev.* **138**, A1112 (1965).
- [7] A. A. Abrikosov, Electron scattering on magnetic impurities in metals and anomalous resistivity effects, *Phys. Phys. Fiz.* **2**, 5 (1965).
- [8] A. P. Klein, New Calculation of the magnetic susceptibility for the Takano-Ogawa theory of Kondo's effect in dilute alloys, *Phys. Rev.* **172**, 520 (1968).
- [9] M. D. Daybell and W. A. Steyert, Localized magnetic impurity states in metals: Some experimental relationships, *Rev. Mod. Phys.* **40**, 380 (1968).
- [10] M.-S. Choi, M. Lee, K. Kang, and W. Belzig, Kondo effect and Josephson current through a quantum dot between two superconductors, *Phys. Rev. B* **70**, 020502(R) (2004).
- [11] R. Maurand, T. Meng, E. Bonet, S. Florens, L. Marty, and W. Wernsdorfer, First-order  $0-\pi$  quantum phase transition in the Kondo regime of a superconducting carbon-nanotube quantum dot, *Phys. Rev. X* **2**, 011009 (2012).
- [12] C. Karrasch and V. Meden, Supercurrent and multiple singlet-doublet phase transitions of a quantum dot Josephson junction inside an Aharonov-Bohm ring, *Phys. Rev. B* **79**, 045110 (2009).
- [13] M. Lee, T. Jonckheere, and T. Martin, Josephson effect through an isotropic magnetic molecule, *Phys. Rev. Lett.* **101**, 146804 (2008).
- [14] S. Li, N. Kang, P. Caroff, and H. Q. Xu,  $0-\pi$  phase transition in hybrid superconductor-InSb nanowire quantum dot devices, *Phys. Rev. B* **95**, 014515 (2017).
- [15] L. Yu, Bound state in superconductors with paramagnetic impurities, *Acta Phys. Sin.* **21**, 75 (1965).
- [16] H. Shiba, Classical spins in superconductors, *Prog. Theor. Phys.* **40**, 435 (1968).
- [17] A. I. Rusinov, Superconductivity near a paramagnetic impurity, *Pis'ma Zh. Eksp. Teor. Fiz.* **9**, 146 (1968) [*JETP Lett.* **9**, 85 (1969)].
- [18] R. Žitko, J. S. Lim, R. López, and R. Aguado, Shiba states and zero-bias anomalies in the hybrid normal-superconductor Anderson model, *Phys. Rev. B* **91**, 045441 (2015).
- [19] S. Pradhan and J. Fransson, Yu-Shiba-Rusinov states of a single magnetic molecule in an  $s$ -wave superconductor, *Phys. Rev. B* **102**, 085136 (2020).
- [20] E. J. H. Lee, X. Jiang, M. Houzet, R. Aguado, C. M. Lieber, and S. D. Franceschi, Spin-resolved Andreev levels and parity crossings in hybrid superconductor-semiconductor nanostructures, *Nat. Nanotechnol.* **9**, 79 (2014).
- [21] A. Costa, J. Fabian, and D. Kochan, Connection between zero-energy Yu-Shiba-Rusinov states and  $0-\pi$  transitions in magnetic Josephson junctions, *Phys. Rev. B* **98**, 134511 (2018).
- [22] G. O. Steffensen, J. C. Estrada Saldaña, A. Vekris, P. Krogstrup, K. Grove-Rasmussen, J. Nygård, A. L. Yeyati, and J. Paaske, Direct transport between superconducting subgap states in a double quantum dot, *Phys. Rev. B* **105**, L161302 (2022).
- [23] M. Leijnse and K. Flensberg, Introduction to topological superconductivity and Majorana fermions, *Semicond. Sci. Technol.* **27**, 124003 (2012).
- [24] J. Alicea, New directions in the pursuit of Majorana fermions in solid state systems, *Rep. Prog. Phys.* **75**, 076501 (2012).
- [25] S. Nadj-Perge, I. K. Drozdov, J. Li, H. Chen, S. Jeon, J. Seo, A. H. MacDonald, B. A. Bernevig, and A. Yazdani, Observation of Majorana fermions in ferromagnetic atomic chains on a superconductor, *Science* **346**, 602 (2014).
- [26] Y. Oreg, G. Refael, and F. von Oppen, Helical liquids and Majorana bound states in quantum wires, *Phys. Rev. Lett.* **105**, 177002 (2010).
- [27] V. Mourik, K. Zuo, S. M. Frolov, S. R. Plissard, E. P. A. M. Bakkers, and L. P. Kouwenhoven, Signatures of Majorana fermions in hybrid superconductor-semiconductor nanowire devices, *Science* **336**, 1003 (2012).
- [28] T. D. Stanescu and S. Tewari, Majorana fermions in semiconductor nanowires: Fundamentals, modeling, and experiment, *J. Phys.: Condens. Matter* **25**, 233201 (2013).
- [29] B. Braunecker and P. Simon, Interplay between classical magnetic moments and superconductivity in quantum one-dimensional conductors: Toward a self-sustained topological Majorana phase, *Phys. Rev. Lett.* **111**, 147202 (2013).
- [30] M. M. Vazifeh and M. Franz, Self-organized topological state with Majorana fermions, *Phys. Rev. Lett.* **111**, 206802 (2013).
- [31] H. Kim, A. Palacio-Morales, T. Posske, L. Rózsa, K. Palotás, L. Szunyogh, M. Thorwart, and R. Wiesendanger, Toward tailoring Majorana bound states in artificially constructed magnetic atom chains on elemental superconductors, *Sci. Adv.* **4**, 5 (2018).
- [32] P. Beck, B. Nyári, L. Schneider, L. Rózsa, A. Lászlóffy, K. Palotás, L. Szunyogh, B. Ujfalussy, J. Wiebe, and R. Wiesendanger, Search for large topological gaps in atomic spin chains on proximitized superconducting heavy-metal layers, *Commun. Phys.* **6**, 83 (2023).
- [33] J. Klinovaja, P. Stano, A. Yazdani, and D. Loss, Topological superconductivity and Majorana fermions in RKKY systems, *Phys. Rev. Lett.* **111**, 186805 (2013).
- [34] S. Körber, B. Trauzettel, and O. Kashuba, Collective Yu-Shiba-Rusinov states in magnetic clusters at superconducting surfaces, *Phys. Rev. B* **97**, 184503 (2018).
- [35] A. Odobesko, D. D. Sante, A. Kowalski, S. Wilfert, F. Friedrich, R. Thomale, G. Sangiovanni, and M. Bode, Observation of tunable single-atom Yu-Shiba-Rusinov states, *Phys. Rev. B* **102**, 174504 (2020).
- [36] F. Friedrich, R. Boshuis, M. Bode, and A. Odobesko, Coupling of Yu-Shiba-Rusinov states in one-dimensional chains of Fe atoms on Nb(110), *Phys. Rev. B* **103**, 235437 (2021).
- [37] A. Villas, R. L. Klees, G. Morrás, H. Huang, C. R. Ast, G. Rastelli, W. Belzig, and J. C. Cuevas, Tunneling processes between Yu-Shiba-Rusinov bound states, *Phys. Rev. B* **103**, 155407 (2021).
- [38] H. Ding, Y. Hu, M. T. Randeria, and A. Yazdani, Tuning interactions between spins in a superconductor, *Proc. Natl. Acad. Sci. USA* **118**, e2024837118 (2021).
- [39] H.-N. Xia *et al.*, Spin-orbital Yu-Shiba-Rusinov states in single Kondo molecular magnet, *Nat. Commun.* **13**, 6388 (2022).
- [40] M. S. Choi, R. López, and R. Aguado, SU(4) Kondo effect in carbon nanotubes, *Phys. Rev. Lett.* **95**, 067204 (2005).
- [41] Y. Okazaki, S. Sasaki, and K. Muraki, Spin-orbital Kondo effect in a parallel double quantum dot, *Phys. Rev. B* **84**, 161305(R) (2011).
- [42] H. Potts, M. Leijnse, A. Burke, M. Nilsson, S. Lehmann, K. A. Dick, and C. Thelander, Selective tuning of spin-orbital Kondo

- contributions in parallel-coupled quantum dots, *Phys. Rev. B* **101**, 115429 (2020).
- [43] K. P. Wójcik and J. Kroha, Quantum spin liquid in an RKKY-coupled two-impurity Kondo system, *Phys. Rev. B* **107**, L121111 (2023).
- [44] O. Kürtössy, Z. Scherübl, G. Fülöp, I. E. Lukács, T. Kanne, J. Nygård, P. Makk, and S. Csonka, Andreev molecule in parallel InAs nanowires, *Nano Lett.* **21**, 7929 (2021).
- [45] N. Banerjee, J. W. A. Robinson, and M. G. Blamire, Reversible control of spin-polarized supercurrents in ferromagnetic Josephson junctions, *Nat. Commun.* **5**, 4771 (2014).
- [46] E. Bhatia, A. Srivastava, J. Devine-Stoneman, N. A. Stelmashenko, Z. H. Barber, J. W. A. Robinson, and K. Senapati, Nanoscale domain Wall engineered spin-triplet Josephson junctions and SQUID, *Nano Lett.* **21**, 3092 (2021).
- [47] A. Vekris, J. C. Estrada Saldaña, T. Kanne, M. Marnauza, D. Olsteins, F. Fan, X. Li, T. H. Olsen, X. Qiu, H. Xu, J. Nygård, and K. Grove-Rasmussen, Josephson junctions in double nanowires bridged by in-situ deposited superconductors, *Phys. Rev. Res.* **3**, 033240 (2021).
- [48] K. Grove-Rasmussen, G. Steffensen, A. Jellinggaard, M. H. Madsen, R. Žitko, J. Paaske, and J. Nygård, Yu-Shiba-Rusinov screening of spins in double quantum dots, *Nat. Commun.* **9**, 2376 (2018).
- [49] H. Schmid, J. F. Steiner, K. J. Franke, and F. von Oppen, Quantum Yu-Shiba-Rusinov dimers, *Phys. Rev. B* **105**, 235406 (2022).
- [50] Z. Scherübl, G. Fülöp, J. Gramich, A. Pályi, C. Schönenberger, J. Nygård, and S. Csonka, From Cooper pair splitting to non-local spectroscopy of a Shiba state, *Phys. Rev. Res.* **4**, 023143 (2022).
- [51] R. Bulla, T. A. Costi, and T. Pruschke, Numerical renormalization group method for quantum impurity systems, *Rev. Mod. Phys.* **80**, 395 (2008).
- [52] M. Žonda, P. Zalom, T. Novotný, G. Loukeris, J. Bätge, and V. Pokorný, Generalized atomic limit of a double quantum dot coupled to superconducting leads, *Phys. Rev. B* **107**, 115407 (2023).
- [53] J. Bauer, A. Oguri, A. C. Hewson, J. Bauer *et al.*, Spectral properties of locally correlated electrons in a Bardeen-Cooper-Schrieffer superconductor, *J. Phys.: Condens. Matter* **19**, 486211 (2007).
- [54] J. C. Estrada Saldaña, A. Vekris, G. Steffensen, R. Žitko, P. Krogstrup, J. Paaske, K. Grove-Rasmussen, and J. Nygård, Supercurrent in a double quantum dot, *Phys. Rev. Lett.* **121**, 257701 (2018).
- [55] S.-H. Ji, T. Zhang, Y.-S. Fu, X. Chen, X.-C. Ma, Jia Li, W.-H. Duan, J.-F. Jia, and Q. Xue, High-Resolution scanning tunneling spectroscopy of magnetic impurity induced bound states in the superconducting gap of Pb thin films, *Phys. Rev. Lett.* **100**, 226801 (2008).
- [56] R. Deacon, A. Oiwa, J. Sailer *et al.*, Cooper pair splitting in parallel quantum dot Josephson junctions, *Nat. Commun.* **6**, 7446 (2015).
- [57] A. Jellinggaard, K. Grove-Rasmussen, M. H. Madsen, and J. Nygård, Tuning Yu-Shiba-Rusinov states in a quantum dot, *Phys. Rev. B* **94**, 064520 (2016).
- [58] R. Žitko and T. Pruschke, Energy resolution and discretization artifacts in the numerical renormalization group, *Phys. Rev. B* **79**, 085106 (2009).
- [59] R. Žitko and J. Bonča, Multiple-impurity Anderson model for quantum dots coupled in parallel, *Phys. Rev. B* **74**, 045312 (2006).
- [60] R. M. Fye, Quantum Monte Carlo study of the one-dimensional symmetric Anderson lattice, *Phys. Rev. B* **41**, 2490 (1990).
- [61] H. Huang, R. Drost, J. Senkpiel *et al.*, Quantum phase transitions and the role of impurity-substrate hybridization in Yu-Shiba-Rusinov states, *Commun. Phys.* **3**, 199 (2020).
- [62] T. Cookmeyer and S. D. Sarma, Engineering the Kitaev spin liquid in a quantum dot system, *Phys. Rev. Lett.* **132**, 186501 (2024).
- [63] A. Bordin, X. Li, D. van Driel, J. C. Wolff, Q. Wang, S. L. D. ten Haaf, G. Wang, N. van Loo, L. P. Kouwenhoven, and T. Dvir, Crossed Andreev reflection and elastic cotunneling in three quantum dots coupled by superconductors, *Phys. Rev. Lett.* **132**, 056602 (2024).
- [64] V. V. Ryazanov, V. A. Oboznov, A. V. Veretennikov, and A. Yu. Rusanov, Intrinsically frustrated superconducting array of superconductor-ferromagnet-superconductor  $\pi$  junctions, *Phys. Rev. B* **65**, 020501(R) (2001).
- [65] A. A. Golubov, M. Yu. Kupriyanov, and E. Il'ichev, The current-phase relation in Josephson junctions, *Rev. Mod. Phys.* **76**, 411 (2004).
- [66] G.-H. Ding, C. K. Kim, and K. Nahm, Fano resonance in electron transport through parallel double quantum dots in the Kondo regime, *Phys. Rev. B* **71**, 205313 (2005).
- [67] A. Wong, W. Brian Lane, L. G. G. V. Dias da Silva, K. Ingersent, N. Sandler, and S. E. Ulloa, Signatures of quantum phase transitions in parallel quantum dots: Crossover from local moment to underscreened spin-1 Kondo physics, *Phys. Rev. B* **85**, 115316 (2012).